Validation of an analytical model of groundwater velocity based on laboratory test and numerical simulation

Jie Ren (renjie@xaut.edu.cn)
Xi'an University of Technology
Jinjin Zhang
Xi'an University of Technology
Dabo Wang
Xi'an University of Technology

Research Article

Keywords: surface water-groundwater exchange, Laboratory test, Temperature field, Seepage field, Analytical model

Posted Date: August 5th, 2022

DOI: https://doi.org/10.21203/rs.3.rs-1919676/v1

Additional Declarations: No competing interests reported.

Version of Record: A version of this preprint was published at Environmental Earth Sciences on May 15th, 2023. See the published version at https://doi.org/10.1007/s12665-023-10959-3.

Abstract

Surface water-groundwater exchange affects the material and energy transfer of rivers and adjacent riparian zones. As an intuitive carrier of energy, temperature can effectively reflect the Spatio-temporal changes the surface water-groundwater exchange process. In this paper, the influence of water head variation and sand sample uniformity on its temperature field and seepage field is studied through a one-dimensional sand column laboratory test. Compare the vertical seepage velocities measured in laboratory tests with the vertical underflow exchange rate calculated by the four analytical models to verify the accuracy of the one-dimensional vertical heat analytical model. The results show that the Hatch analytical solution, Keery analytical solution, McCallum analytical solution and Luce analytical solution calculated by VFLUX2 through MATLAB are reliable for calculating the vertical undercurrent exchange rate of the heterogeneous sand column.

1. Introduction

As one of the most crucial water resources on earth, rivers have always been the focus of research in the fields of hydraulic engineering, environmental engineering, and earth science, especially the relationship between surface water and groundwater (Dun et al., 2014; Kanduč et al., 2014; Lu et al., 2018) are gaining importance in water resource management policies. Continuous, dynamic interactions between these two water bodies sustain the biogeochemical and ecological processes at the water-groundwater interface in rivers, lakes, and wetlands (Masaki et al., 2002; Vogt et al., 2012), and these dynamic interactions occur mainly in the subsurface of the riverbed and riparian zone, where water flows across the riverbed and banks into shallow subsurface flow paths and back into the river (Trauth et al., 2013; Kiel and Cardenas., 2014; Lane et al., 2018; Chow et al., 2019; Lu et al., 2020), this process is always accompanied by the transport and exchange of water, heat and solute, which is very important for flood storage, Significant impact on water quality and ecosystem health(Qureshi and Harrison., 2001; Wilding et al., 2014; Swanson et al., 2017).

Irrigation water in rivers, streams, lakes, wetlands, irrigation water in bare canals, offshore seawater and other porous media passing through the bottom of water bodies will exchange with groundwater in most cases. The exchange process between surface water and groundwater is always accompanied by the transfer and exchange of energy. Among them, temperature, as an intuitive carrier of power, is a characterization factor that can reflect the temporal and spatial changes in the undercurrent exchange process. Because of its easy observation and no pollution, it has certain advantages as a natural tracer (Engelhardt et al., 2011; Engelhardt et al., 2013). In recent years, the development of comprehensive computer coding has made it easy to obtain large temperature time series recordings various sites and at multiple depths (Swanson and Cardenas., 2010; Gordon et al., 2012). Applying a 1D heat transport model to a high-resolution temperature time-series dataset collected using distributed temperature sensing (DTS) enabled the mapping of the spatial variation of vertical flux with depth (Vogt et al., 2010). Automated computational methods have facilitated the more flexible recording of high-resolution DTS temperature data to characterize fine-scale variations in depth-dependent flux at multiple sites (Fritz and

Arntzen., 2007; Gordon et al., 2012). Exchange rates are derived from temperature time series generated by groundwater and heat transport (Cardenas, 2010; Laura et al., 2010). Vogt et al. (2012) used distributed optical fiber temperature sensors (DTS) to continuously observe the temperature of shallow groundwater in the riparian zone. By analyzing the temperature time series of the vertical section, they found that the groundwater temperature in the riparian zone is not spatially related. Uniform distribution, but non-uniform distribution with groundwater velocity at different depths. Chen (2020) Uses the real-time monitoring data of water temperature and water level to study the distribution characteristics of the temperature field of the subsurface layer in the riparian zone in different seasons and different spatial locations, and uses the water temperature data to calculate the groundwater flow rate by the Hatch amplitude method and the COMOSL Multiphysics numerical solution method Comparison of the computed results: Although the two are different in magnitude, the overall variation law of the computed results is the same. Zhu et al. (2013) used the river bed temperature as a tracer variable, based on the analytical solution of the one-dimensional steady-state vertical heat transport problem, and revealed through continuous monitoring of the temperature of different vertical profiles of the river bed in the field. The distribution law of the depth of the undercurrent zone. Ji et al. (2018) took the continental beach in the Manwan Reservoir area of the Lancang River as the research object. The monitored the changes in water level and water temperature in the monitoring well of the continental beach in real-time during the operation of the reservoir. Method and temperature tracer method to calculate the flow rate. Scholars such as Dylan et al. (2015) used the sand column test, adopted the one-dimensional heat transport theory, and studied the exchange volume between surface water and groundwater through the temperature amplitude ratio and phase difference; Landon et al. (2016) analyzed the measured temperature data by arranging temperature sensors and using the one-dimensional heat transport theory in field experiments, and concluded that the method of calculating seepage velocity using the amplitude method is the most reliable method for calculating seepage velocity in the subsurface zone; Conant (2004) identified the existence of the sub current area and delineated the scope of the subsurface zone by the temperature tracing method; Alexander et al. (2010) and Briggs et al. (2012) adopted the temperature tracing method, the water exchange between surface water and groundwater in the subsurface zone was calculated through the temperature data of continuous dynamic monitoring, and the relevant hydrogeological parameters in the area were estimated. Wondzell et al. (1996) quantitatively studied the undercurrent convection flow and groundwater inflow in river gravel ridges by monitoring data from field experiments and establishing groundwater models. The basic theory of the exchange of undercurrents in the riverbed was established.

Surface water-groundwater exchange rates vary significantly in time and space, making them difficult to quantify, especially at the multi-spatial and long-term resolution required for many field applications (Kalbus et al., 2006; Fritz and Arntzen., 2007; Fanelli and Lautz., 2008; Briggs et al., 2012). With the accumulation of riverbed sediments over time, the surface water-groundwater exchange rate is affected by solar radiation and air temperature, and the temperature field of river surface water and undercurrent zone has the characteristics of diurnal, monthly and seasonal fluctuations (Kasahara and Hill., 2006; Rosenberry and Pitlick., 2009). Phenomena such as melting snow, blizzard, tide, and reservoir operation

are the main factors that cause the water level fluctuation in the river reach. Fluctuating of the river water level is an important factor in the confluence of river water and groundwater in the riparian zone. Along with the change of the upstream river flow, the river water level fluctuates. The fluctuation of the water level increases the wetting area of the riparian zone and thus expands the range of river water and riparian groundwater exchange (Taniguchi., 2003; Harvey et al., 2013); such fluctuations contribute to the changing hydraulic gradient between river water and groundwater, increasing the rate of surface water-groundwater exchange (Edwardson et al., 2003). In the past few years, there have been some notable advances in the application of 1D heat transport models for surface water-groundwater exchange, and there are many practical examples of applying these results (Fanelli and Lautz., 2008; Anderson et al., 2010; Lautz et al., 2010). Hatch et al. (2006) and Keery et al. (2007) applied a one-dimensional heat transfer model to infer surface water-groundwater exchange rates from records of subsurface temperature over time.

Through the research of many scholars above, we found that the existing research is to obtain a relatively accurate one-dimensional vertical heat analytical model by comparing the analytical solution of the one-dimensional vertical heat transport problem with the numerical solution obtained by the hydraulic method. Still, there is a lack of Corresponding test verification. Therefore, in this paper, aiming at the one-dimensional thermal migration analytical model, a one-dimensional homogeneous sand column laboratory test is carried out to simulate the water head change through the laboratory test, and the effect of the water level rising and falling process on the temperature field of the homogeneous and heterogeneous sand column is studied. And seepage field effects. Comparing the temperature data measured in the laboratory test to calculate the groundwater flow rate and the groundwater flow rate obtained from the measured seepage amount, the vertical seepage velocity measured in the laboratory test is compared with the vertical underflow exchange rate calculated by the four analytical models, to verify the one-dimensional vertical flow rate the accuracy of the thermal analysis model.

2 Methods

Surface water-groundwater exchange rates vary significantiy in time and space, making them difficult to quantify, especially at the multi-spatial and long-term resolution required for many field applications (Kalbus et al., 2006; Fritz and Arntzen., 2007; Fanelli and Lautz., 2008; Briggs et al., 2012) Hatch et al. (2006) and Keery et al. (2007) apply a one-dimensional heat transfer model Surface water-groundwater exchange rates are derived from recordings of subsurface temperature over time. The existing research is to obtain a more accurate one-dimensional vertical heat analysis model by comparing the analytical solution of the one-dimensional vertical heat transport problem with the numerical solution obtained by hydraulic methods, but the corresponding experimental verification is lacking. Therefore, in this paper, by comparing the simulated water head changes in the laboratory test. The groundwater flow rate calculated by the measured temperature data is compared with the groundwater flow rate obtained by the measured water infiltration to verify the accuracy of the one-dimensional vertical thermal analysis model.

2.1 One-dimensional thermal transport equation

The exchange modes of heat transport in surface water-groundwater exchange mainly consist of two modes: heat conduction (heat transfer through solids in sediments and water flow) and thermal convection (heat transfer through water flow).

Stellman (1963) assumed that the geologic body was saturated homogeneous isotropic porous medium; In porous media, solid-liquid two-phase transport is isotropic, where water flow is stable, and heat transport is variable. The solid phase skeleton and pore fluid are in a state of local thermal equilibrium, and their thermal characteristics remain unchanged in time and space. A fundamental equation describing the transport of water and heat in saturated porous media is proposed (Shanafield et al., 2011). Therefore, the mathematical model of heat transport in the subsurface flow zone is as follows:

$$\frac{\partial^2 T}{\partial x^2}+\frac{\partial^2 T}{\partial y^2}+\frac{\partial^2 T}{\partial z^2}-\frac{\rho_w C_w}{\lambda}\left(u_x\frac{\partial T}{\partial x}+u_y\frac{\partial T}{\partial y}+u_z\frac{\partial T}{\partial z}\right)=\frac{\rho C}{\lambda}\frac{\partial T}{\partial t}$$

1

In the formula, T is the temperature (°C); t is time (s); ρ_w and C_w are the density (kg/m^3) and mass heat capacity (J/kg·°C) of water, respectively; ρ and C are saturated porous media, respectively The equivalent density (kg/m^3) and equivalent mass heat capacity (J/kg °C) of; u_x u_y and u_z are the seepage velocity (m/s) in the x y and z directions; λis the saturated porous medium The equivalent thermal conductivity of (w/(m s)).

In addition, due to the complex structure of the undercurrent zone, the surface water-groundwater exchange has a high degree of variability in time and space (Vogt et al., 2010; Liu Dongsheng et al., 2017). In addition to the overall material properties of saturated porous media, the exchange rate also needs to comprehensively consider the effects of seasons, rainfall, solar radiation, and snowfall (Song et al., 2019).

In 1965, Stallman (1965) basis on the hypothesis in the porous media flow in one-dimensional vertically non-uniform stable migration, the equivalent density of saturated porous media, the equivalent mass heat capacity and equivalent heat transfer coefficient according to the principle to determine the average volume, one-dimensional heat transport equation are presented (Lautz, 2012), and through the method of undetermined coefficients is given an analytical solution, The specific expression is:

$$T-T_0=A\mathrm{e}^{-az}\sin\left(\frac{2\pi t}{P}-bz\right)$$

2

$$a=\left[\left(K^2+\frac{V^4}{4}\right)^{1/2}+\frac{V^2}{2}\right]^{1/2}-V$$

3

$$b = \left[\left(K^2 + \frac{V^4}{4} \right)^{1/2} - \frac{V^2}{2} \right]^{1/2}$$

4

In the formula, $K = \rho C\pi / Pk$; $V = \rho_w C_w u_z / 2\lambda$; a and b are constants.

2.2 Existing models

Stallman's pioneering work laid the foundation for subsequent developments in the field of surface and groundwater exchange. Many later scholars have improved the Stallman analytical model in light of the actual situation on the basis of the improvement of computer data processing performance and the innovation of temperature measurement instruments and acquisition methods. The improved model is more suitable for complex boundary conditions and hydrogeological environments (Lautz, 2012).

(1) Hatch solution

Hatch et al. (2006) conducted in-depth research on the Stallman analysis method and believed that:

$$T(z,t) = A \exp\left(\frac{\upsilon_t z}{2k_e} - \frac{z}{2k_e}\sqrt{\frac{\alpha + \upsilon_t^2}{2}} \right) \cos\left(\frac{2\pi t}{P} - \frac{z}{2k_e}\sqrt{\frac{\alpha - \upsilon_t^2}{2}} \right)$$

5

In the formula,

$$\alpha = \sqrt{\upsilon_t^4 + (8\pi k_e / P)^2}$$

6

υ_t is the temperature front-end movement speed (m/s).

$$\upsilon_t = u_z \frac{\rho_w C_w}{\rho C}$$

7

The right side of Eq. (5) represents the changes in the amplitude and phase of temperature fluctuations with the increase of sediment depth, respectively. Hatch et al. (2006) divided Eq. (5) into two components and solved the amplitude and phase of the temperature between the measurement points at two different depths, respectively thus obtaining:

$$A_r = \exp\left\{ \frac{\Delta z}{2k_e}\left(u_z - \sqrt{\frac{\alpha + v_t^2}{2}} \right) \right\}$$

8

$$\Delta\varphi = \frac{P\Delta z}{4\pi k_e}\sqrt{\frac{\alpha - v_t^2}{2}}$$

9

$$u_{zA_r} = \frac{\rho C}{\rho_w C_w}\left(\frac{2k_e}{\Delta z}\ln A_r + \sqrt{\frac{\alpha + v_t^2}{2}} \right)$$

10

$$\left| u_{z\Delta\varphi} \right| = \frac{\rho C}{\rho_w C_w}\sqrt{\alpha - 2\left(\frac{4\pi\Delta\varphi k_e}{P\Delta z} \right)^2}$$

11

In the formula: u_{zAr} and $u_{z\Delta\varphi}$ are the vertical groundwater seepage velocity (m/s) calculated from the amplitude and phase respectively; Δz is the vertical distance of the temperature monitoring point (m); A_r is the temperature amplitude A_d of the deeper measurement point The ratio of the temperature measurement point amplitude A_s at the shallow measurement point, As that is, A_r=A_d/A_s (as shown in Fig. 1b); $\Delta\varphi$ is the phase difference between the two monitoring points, which is the time lag (s). In Fig. 1, a represents a schematic diagram of the layout of common temperature monitoring instruments, and b represents the temperature time series temperature measurement curve of the deep and shallow measurement points.

(Fig. 1)

(2) Keery solution

Keery et al. (2007) ignored the effect of thermal dispersion on heat transport in porous media, improved the Stallman model, and gave the analytical solution of one-dimensional heat transport equation:

$$\left(\frac{H^3 \ln A_r}{4\Delta z} \right) u_{zA_r}^3 - \left(\frac{5H^2 \ln^2 A_r}{4\Delta z^2} \right) u_{zA_r}^2 + \left(\frac{2H \ln^3 A_r}{\Delta z^3} \right) u_{zA_r} + \left(\frac{\pi\rho c}{\lambda P} \right)^2 - \frac{\ln^4 A_r}{\Delta z^4} = 0$$

12

$$|u_{z\Delta\varphi}| = \sqrt{\left(\frac{\rho C \Delta z}{\rho_w C_w \Delta\varphi}\right)^2 + \left(\frac{4\pi\Delta\varphi\lambda}{\rho_w C_w P \Delta z}\right)^2}$$

13

in the formula: $H = \rho_w C_w/\lambda$

(3) McCallum solution

Although the Hatch analytical method and the Keery analytical method can calculate the vertical seepage velocity relatively accurately, there is a certain difference between the vertical seepage velocity calculated by the amplitude ratio method and the phase lag method. The calculation results are affected by the thermophysical parameters of the porous medium, and the thermophysical parameters have certain uncertainties, which have a significant impact on the accuracy of the analytical model (Shanafield et al., 2011; Rau, 2012).

In response to the above problems, McCallum et al. (2012) combined the amplitude ratio equation and the phase lag equation in the Hatch solution to obtain the following equation:

$$u_{zA_r\Delta\varphi} = -\frac{\rho C}{\rho_w C_w}\left(\frac{\Delta Z\left(P^2\ln^2 A_r - 4\pi^2\Delta\varphi^2\right)}{\Delta\varphi\sqrt{16\pi^4\Delta\varphi^4 + 8P^2\pi^2\Delta\varphi^2\ln^2 A_r + P^4\ln^4 A_r}}\right)$$

14

$$k_e = \frac{\Delta z^2 P^2 \ln A_r\left(4\pi^2\Delta\phi^2 - P^2\ln^2 A\right)}{\Delta\phi\left(P^2\ln^2 A_r + 4\pi^2\Delta\phi^2\right)\left(P^2\ln^2 A_r - 4\pi^2\Delta\phi^2\right)}$$

15

Where: $u_{zAr\varphi}$ is the vertical seepage velocity (m/s) calculated by the amplitude-phase combination method.

(4) Luce solution

Luce et al. (2013) The values of parameters a and b in the undetermined coefficients of the Stallman analytical solution can be approximately expressed as the amplitude ratio and phase lag of the day-night temperature signal divided by the vertical distance between the measuring points, namely:

$$a \approx \frac{-\ln\left(\frac{A_d}{A_s}\right)}{z_d - z_s} = \frac{-\ln\left(\frac{A_d}{A_s}\right)}{\Delta z} = \frac{-\ln \mathrm{A}_r}{\Delta z}$$

16

$$b \approx \frac{\varphi_d - \varphi_s}{z_d - z_s} = \frac{\Delta\varphi}{\Delta z}$$

17

And from this, it follows:

$$u_{zA_r\Delta\varphi} = \frac{\rho C}{\rho_w C_w}\left(\frac{\omega\Delta \mathrm{z}}{\Delta\varphi}\left(\frac{1-\eta^2}{1+\eta^2}\right)\right) = \frac{\rho c}{\rho_w c_w}\left(\frac{\eta\omega\Delta \mathrm{z}}{-\ln A_r}\left(\frac{1-\eta^2}{1+\eta^2}\right)\right)$$

18

$$k_e = \frac{\omega\Delta z^2}{\Delta\phi^2\left(\frac{1}{\eta}+\eta\right)} = \frac{\omega\eta^2\Delta z^2}{\ln^2 A_r\left(\frac{1}{\eta}+\eta\right)}$$

19

in the formula: η=-lnA_r/$\Delta\varphi$; ω = 2π/P, in here k_e = λ/ρC.

2.3 One-dimensional sand column test

2.3.1 Test Apparatus

The test device consists of a plexiglass water tube, a high-precision temperature sensor (Omega), a water pump, a data collector, a computer, a measuring cup, an electronic scale, a rubber tube, a heating rod, a water bucket and a sand column. The plexiglass water pipe is divided into upper and lower parts, the inner diameter is 10 cm, the outer diameter is 12 cm, the upper length is 100 cm, and the lower length is 20 cm, which is connected by column-shaped connecting sections. The upper plexiglass water pipe is arranged every 10 cm from 5 cm above the bottom. The temperature sensor is arranged with a filter gauze at the bottom, the fine sand prepared in advance is placed, and the temperature sensor is compacted and placed at an interval of 10 cm. The height of the sand column is 70 cm. There are three water outlets and one water inlet above the sand column. The water in the bucket is heated by the heating rod, and the water flows from the bucket into the water pipe by the water pump, and flows into the bucket through the water outlet at different heights to form stable circulating water. A water outlet is set at the lower part, and the amount of water seeping from the sand column is measured. The purpose of the rubber hose is to connect the water pump, bucket, and plexiglass hose and to receive the water seeping out from the sand column. The schematic diagram of the test device is shown in Fig. 2.

(Fig. 2)

2.3.2 Test method

Using sand column experiment, a one-dimensional flow of water and heat is generated in the porous medium. The upper end of the sand column is provided with a water flow with quasi-sinusoidal temperature change by a heating rod. Before the test began, the sand column was saturated with water flow through the sand column for several days until the flow measured by the measuring cup stabilized and the sand column had a uniform temperature distribution. The experiments were carried out for two different water head changes (rising and falling), two different soil types (homogeneous and heterogeneous), three different water heads (10 cm, 20 cm and 35 cm) and sinusoidal temperature changes. The test plan is shown in Table 1.

(Table 1)

Plan 1: The water pump provided tap water with an initial temperature of 22°C to the plexiglass water pipe through the water inlet. The rubber pipe with the 35 cm water outlet was placed in the bucket to form a circulating water with a water head of 35 cm. When the water output from the bottom water outlet is stable, the temperature of the bucket is heated by the heating rod, and the temperature data is read by the data collector. When the bucket is full of water through the pre-experiment, it takes 15 minutes to heat 1 ℃, and the heating is continued for 2 hours, so that The water temperature of the bucket was raised to 30°C; after that, ice cubes were added to reduce the water temperature of the water bucket by 1°C every 15 minutes, and a quasi-sinusoidal temperature oscillating water head from 22°C to 30°C was provided to the upper end of the sand column. After that, put away the rubber tube of the 35 cm water outlet, and put the rubber tube of the 20 cm water outlet in the bucket to form circulating water with a head of 20 cm; after the water temperature is heated and cooled, put away the rubber tube of the 20 cm water outlet. Place the rubber tube of the 10 cm water outlet in the bucket to form circulating water with a head of 35 ~ 20 ~ 10 cm. Over time, by collecting the flow from the water outlet in the measuring cup, the measuring cup is placed on the electronic scale, the electronic scale data is read and recorded every 2 minutes, and the water is poured back into the bucket when the measuring cup is full, the weight is recorded by the weight every 2 minutes Variation data to solve for the actual seepage velocity in the vertical direction of the sand column, and the obtained velocity is the midpoint velocity of the two measurement intervals; for example, if the velocity is measured between 1 minute and 3 minutes, the velocity is the instantaneous velocity at 2 minutes flow rate.

Plan 2: The water pump provided tap water with an initial temperature of 22°C to the plexiglass water pipe through the water inlet. The rubber pipe with the 10 cm water outlet was placed in the bucket to form a circulating water with a head of 10 cm. When the water output from the bottom outlet was stable, the temperature data was recorded, and the heating rod continued to heat for 2 hours, so that the water temperature of the bucket rose to 30°C; after that, ice cubes were added to reduce the water temperature of the water bucket by 1°C every 15 minutes, Quasi sinusoidal temperature oscillation from 22°C to 30 ℃ for 4 hours is generated. After that, put away the rubber tube of the 10 cm water outlet, and put the rubber tube of the 20 cm water outlet in the bucket to form circulating water with a head of 20 cm; after heating and cooling, put away the rubber tube of the 20 cm water outlet, Place the rubber tube with the 35 cm water outlet in the bucket to form circulating water with a head of 10 ~ 20 ~ 35 cm.

Plan 3: The upper 10 cm of fine sand is dug out and filled with coarse sand of equal height. The water pump provides tap water with an initial temperature of 22°C to the plexiglass water pipe through the water inlet, and the rubber pipe of the 10 cm water outlet is placed in the bucket. Circulating water with a head of 10 cm was formed. When the water output from the bottom outlet was stable, the temperature of the bucket was controlled by a heating rod, and the temperature of the bucket was continuously heated for 2 hours, rising to 30°C; after that, ice was added to reduce the water temperature of the bucket by 1°C every 15 minutes, resulting in a temperature from 22°C to 30°C for 4 hours. Quasi-sinusoidal temperature oscillations. After that, put away the rubber tube of the 10 cm water outlet, and put the rubber tube of the 20 cm water outlet in the bucket to form circulating water with a head of 20 cm; after heating and cooling, put away the rubber tube of the 20 cm water outlet, Place the rubber tube with the 35 cm water outlet in the bucket to form circulating water with a head of 10 ~ 20 ~ 35 cm.

3 Results And Discussion

For the one-dimensional thermal transport analytical model, the commonly used solvers are VFLUX2 (Gordon et al., 2012)and Ex-Stream (Swanson and Cardenas, 2011). In this experiment, VFLUX2 was used to solve the vertical seepage velocity. VFLUX2 was developed through MATLAB computing language programming. The Hatch analytical solution, Keery analytical solution, McCallum analytical solution and Luce analytical solution can be used to calculate and analyze the vertical seepage velocity of the sand column. Copy the VFLUX program to a folder in the MATLAB search path, import the temperature data, and enter the code “site12 = vfluxformat (aa(:,1), aa(:,2:3), [0.05 0.15])”, aa(:,1)” is a column of sample times; “aa(:,2:3)” is a matrix of temperature sequences; “[0.05 0.15]” is a row vector of depth positions for each sensor, in meters After running VFLUX, enter the code “site12 = vflux(site12, 0, [1 2], 1, 0.41, 0.01, 0.00030, 0.312, 1)”, in the MATLAB command bar after running VFLUX, press the MATLAB command prompt, press Enter to get VFLUX The riparian undercurrent exchange rate calculated by the four analytical models pre-defined in.

Table 2 lists the parameters used by the four analytical models in the VFLUX2 calculation program. The parameters are mainly based on Lautz et al. (2012) and laboratory measurements.

(Table 2)

3.1 Influence of dropping water head of the homogeneous sand column

Figure 3(B) The dotted line represents the temperature amplitude of each monitoring point, and the solid line represents the temperature time series data after filtering. In the real environment, the measured temperature time series data are often superimposed by temperature signals of multiple frequencies and contain various noise signals. The VFLUX2 program can filter natural and human factors through FIR low-pass filter (finite impulse response). High-frequency noise (Lautz, 2012).

In this study, the sand column experiment generates a one-dimensional vertical flow in the sand column. In these one-dimensional flow fields, temperature changes are monitored by temperature sensors at different positions, and the flow velocity at different depths is calculated by VFLUX2. Since the phase method can only calculate the size, the direction cannot be determined, and only the seepage velocity calculated by the amplitude method is considered. The calculation results have the following characteristics: in the flow velocity calculation results of the amplitude method, the flow velocity at 0.1 m is also calculated, and the velocity range value calculated by the Hatch amplitude method is 3.66×10^{-5}-8.85×10^{-5} m/s, The velocity values calculated by the Keery amplitude method are 3.55×10^{-5} 8.18×10^{-5} m/s. For the amplitude-phase combination method, the flow velocity calculated by the McCallum solution and the Luce solution coincide, and the calculated flow velocity value is 7.30×10^{-5} 8.90×10^{-5} m/s, which is larger than that of the amplitude method. When the water head is 35 cm, the measured seepage velocity is about 6.9×10^{-5} m/s; when the water head is 20 cm, the measured seepage velocity is about 5.9×10^{-5} m/s; when the water head is 10 cm, the measured seepage velocity is 5.1×10^{-5} m/s. As the water head decreases, the calculated results of each model gradually decrease. As we can seen that the calculated results of the Hatch amplitude method at 0.1 m are in good agreement with the measured values, which is consistent with the previous research results of Lautz (2012). To compare the groundwater flow velocity at different depths, the seepage velocity calculated by the Hatch amplitude method at 0.10 m, 0.20 m and 0.30 m was selected as the research object figure (3C). The value ratio is relatively small. In the depth direction, the seepage velocity decreases, and the flow velocity at 0.2 m-0.3 m is close to parallel, which is consistent with the field test results of Li et al. (2016) match.

(Fig. 3)

3.2 Influence of rising water head on the homogeneous sand column

Figure 4 shows the vertical temperature and seepage velocity change curves of the homogeneous sand column under the condition of water head rising. From the analysis in the previous section, it can be seen that the vertical flow velocity at 0.1 m is the largest and is in line with the measured flow velocity. Therefore, four analytical models were selected at 0.1 m. The calculated flow rate is compared with the measured flow rate. The velocity values calculated by the Hatch amplitude method are 4.47×10^{-5}~7.73×10^{-5} m/s, and the velocity values calculated by the Keery amplitude method are 3.88×10^{-5}~7.21×10^{-5} m/s. For the amplitude-phase combination method, the flow velocity calculated by the McCallum solution and the Luce solution coincide, and the calculated flow velocity value is 5.61×10^{-5}~8.90×10^{-5} m/s, which is larger than that of the amplitude method. As the water head rises, the calculation results of each model gradually increase. As we can seen that the 0.1m calculation results and the measured values of the four analytical models have high accuracy. The Hatch amplitude method 0.1m calculation results and the measured value have the highest agreement, the Keery amplitude method is too small, and the flow velocity calculated by the McCallum solution and the Luce solution is too large.

(Fig. 4)

3.3 Influence of rising water head o the heterogeneous sand column

From the above analysis: the four analytical models have high accuracy in the calculation results and measured values of the vertical velocity of the homogeneous sand column. The Hatch amplitude method has the highest agreement between the calculated results and the measured values. Figure 5. Change curve of vertical temperature and seepage velocity under the condition of water head rising in the heterogeneous sand column. Because the 0.05 m and 0.15 m temperature sensors are in different sand grains, the flow velocity at 0.2 m is selected for this working condition. The calculated value obtained by the Hatch amplitude method The e velocity value is 9.23×10^{-5}~9.35×10^{-5}m/s, and the velocity value calculated by the Keery amplitude method is 9.01×10^{-5}~9.11×10^{-5} m/s, for the amplitude-phase combination method, the flow velocity calculated by the McCallum solution and the Luce solution coincide, and the calculated flow velocity value is 1.37×10^{-4}~1.38×10^{-4} m/s, which is larger than the amplitude method. When the water head is 10 cm, the measured seepage velocity is about 1.18×10^{-4} m/s; when the water head is 20 cm, the measured seepage velocity is about 1.33×10^{-4} m/s; when the water head is 35 cm, the measured seepage velocity is 1.49×10^{-4} m/s. As we can seen from Fig. 5B that the flow velocity at 0.2 m calculated by the analytical model is smaller than the measured flow velocity, which is consistent with the results of working condition 1. The flow velocity calculated by McCallum solution and Luce solution is the largest, followed by the Hatch amplitude method, and Keery's approach was the lowest.

(Fig. 5)

On the whole, the magnitude of the flow rate calculated by the amplitude ratio method and the amplitude combination method is relatively consistent with the measured flow rate size and the overall change law of the calculated result. Analytical solution, McCallum analytical solution and Luce analytical solution are reliable in analyzing vertical seepage velocity. For the amplitude ratio method, the velocity results calculated by Hatch solution and Keery solution maintain a certain numerical difference. Keery et al. (2007) conducted a comparative analysis of the Hatch solution and the Keery solution, and concluded that the Hatch solution is more accurate than the Keery solution due to the consideration of thermal dispersion effects. From the above analysis, As we can seen that it is more reliable to use the four models to calculate the vertical seepage velocity of the heterogeneous sand column. Therefore, in the subsequent calculation and analysis of the vertical flow velocity of the heterogeneous underflow zone, four analytical models can be used for analysis.

4 Conclusion

In this paper, the temperature data measured by the laboratory test and the measured seepage flow rate are verified by VFLUX2 to calculate and analyze the vertical seepage velocity through four MATLAB

analytical models: Hatch analytical solution, Keery analytical solution, McCallum analytical solution and Luce analytical solution. The main conclusions are as follows:

(1) Three kinds of indoor sand column tests were carried out: the influence of the falling head on the temperature field and seepage field of the homogeneous sand column, the influence of the rise of the water head on the temperature field and seepage field of the homogeneous sand column, and the influence of the rise of the water head on the temperature field and the seepage field of the heterogeneous sand column. The vertical seepage velocity calculated by the measured seepage flow is compared with the solutions of the four analytical models, and the solution of the vertical flow velocity of the analytical model in the heterogeneous underflow zone is analyzed.

(2) Combined with the indoor physical model test, the measured seepage calculated vertical seepage velocity is compared with the Hatch analytical solution, Keery analytical solution, McCallum analytical solution and Luce analytical solution calculated by VFLUX2 by MATLAB. The results show that the computational efficiency of these four analytical models is not high. The vertical seepage velocity of the homogeneous sand column is reliable.

Declarations

Acknowledgements

This work was supported by the Program 2022TD-01 for Shaanxi Provincial Innovative Research Team and the Key Scientific Research Project of the Education Department of Shaanxi Province (Grant No. DFZX202007) and Supported by the Open Research Fund Program of State Key Laboratory of Eco-hydraulics in Northwest Arid Region Xi'an University of Technology (Grant No. 2021KFKT-3), and Supported by Open Research Fund Program of State Key Laboratory of Hydraulics and Mountain River Engineering Sichuan University (Grant No. SKHL2106).

Conflict of interests

The authors declare that are no conflict of interest.

References

1. Dun, Y., Tang, C., Shen, Y. (2014). Identifying interactions between river water and groundwater in the North China Plain using multiple tracers. Environ Earth, 72, 99–110.
2. Kanduč, T., Grassa, F., McIntosh, J. Stibilj, V., Ulrija-Supovec, M., Supovec, L., Jamnikar, S. (2014). A geochemical and stable isotope investigation of groundwater/surface-water interactions in the Velenje Basin, Slovenia. Hydrogeol J 22, 971–984.
3. Lu, C., Chen, S., Jiang, Y., Shi, J., Yao, C., Su, X. (2018). Quantitative analysis of riverbank groundwater flow for the Qinhuai River, China, and its influence factors. Hydrological Processes, 32: 2734–2747.

4. Hayashi, M., Rosenberry, D.O. (2002). Effects of Ground Water Exchange on the Hydrology and Ecology of Surface Water. Ground Water, 40: 309–316.
5. Vogt, T., Schirmer, M., Cirpka, O. A. (2012). Investigating riparian groundwater flow close to a losing river using diurnal temperature oscillations at high vertical resolution, Hydrol. Earth Syst, 16, 473–487.
6. Trauth, N., Schmidt, C., Maier, U., Vieweg, M., Fleckenstein, J. H. (2013). Coupled 3-D stream flow and hyporheic flow model under varying stream and ambient groundwater flow conditions in a pool-riffle system, Water Resour. Res., 49, 5834–5850.
7. Kiel, B., Bayani Cardenas, M. (2014). Lateral hyporheic exchange throughout the Mississippi River network. Nature Geo, 7, 413–417.
8. Lane, Charles R., Leibowitz, Scott G., Autrey, Bradley C., LeDuc, Stephen D., Alexander, Laurie C. (2018). Hydrological, Physical, and Chemical Functions and Connectivity of Non-Floodplain Wetlands to Downstream Waters: A Review. Journal of the American Water Resources Association (JAWRA) 54(2): 346–371.
9. Chow, R., Wu, H., Bennett, J.P., Dugge, J., Wöhling, T., Nowak, W. (2019). Sensitivity of Simulated Hyporheic Exchange to River Bathymetry: The Steinlach River Test Site. Ground Water, 57: 378–391.
10. Lu, C., Ji, K., Zhang, Y., Jan, H. F., Zheng, C., Kate, S. (2020). Event-Driven Hyporheic Exchange during Single and Seasonal Rainfall in a Gaining Stream. Water Resources Management. 34. 1–15.
11. Qureshi, M.E., Harrison, S.R. (2001). A decision support process to compare riparian revegetation options in Scheu Creek catchment in north Queensland. Journal of environmental management, 62 1, 101–102.
12. Thomas K. W., John S., David M., Rood, S., Poff, N. (2014). Riparian responses to reduced flood flows: comparing and contrasting narrowleaf and broadleaf cottonwoods, Hydrological Sciences Journal, 59:3–4, 605–617.
13. Kozlowski, D., Hall, R., Swanson, S., Heggem, D. (2016). Linking Management and Riparian Physical Functions to Water Quality and Aquatic Habitat. Journal of Water Resource and Protection, 8, 797–815.
14. Engelhardt, I., Piepenbrink, M., Trauth, N., Stadler, S., Kludt, C., Schulz, M., Schüth, C., Ternes, T.A. (2011). Comparison of tracer methods to quantify hydrodynamic exchange within the hyporheic zone. Journal of Hydrology, 400, 255–266.
15. Engelhardt, I., Prommer, H., Moore, C.R., Schulz, M., Schüth, C., Ternes, T.A. (2013). Suitability of temperature, hydraulic heads, and acesulfame to quantify wastewater-related fluxes in the hyporheic and riparian zone. Water Resources Research, 49(1):426–440.
16. Swanson, T.E., Cardenas, M.B. (2010). Diel heat transport within the hyporheic zone of a pool-riffle-pool sequence of a losing stream and evaluation of models for fluid flux estimation using heat. Limnology and Oceanography, 55(4):1741–1754.
17. Gordon, R.P., Lautz, L.K., Briggs, M.A., McKenzie, J.M. (2012). Automated calculation of vertical pore-water flux from field temperature time series using the VFLUX method and computer program.

Journal of Hydrology, 420, 142–158.

18. Vogt, T., Schneider, P., Hahn-Woernle, L., Cirpka, O.A. (2010). Estimation of seepage rates in a losing stream by means of fiber-optic high-resolution vertical temperature profiling. Journal of Hydrology, 380, 154–164.
19. Fritz, B., Arntzen, E.V. (2007). Effect of Rapidly Changing River Stage on Uranium Flux through the Hyporheic Zone. Ground Water, 45: 753–760.
20. Cardenas, M.B. (2010). Thermal skin effect of pipes in streambeds and its implications on groundwater flux estimation using diurnal temperature signals. Water Resources Research, 46, W03536.
21. Lautz, L.K. (2010). Impacts of nonideal field conditions on vertical water velocity estimates from streambed temperature time series. Water Resources Research, 46, W01509.
22. Chen, B. (2020). Experimental study on the dynamic change characteristics of hydro-thermal in beach under water level fluctuation.
23. Zhu, S., Shu, C., Lu, P. (2013). Study on the heterogeneity of vertical hyporheic flux using a heat tracing method. Journal of Hydraulic Engineering, (07),818–825.
24. Ji, Y., Shi, W., Chen, Q., An, L. (2018). Calculation method of temperature tracing velocity in the hyporheic zone of the reservoir continent beach. Journal of Water Resources and Water Engineering, (03),159–163.
25. Irvine, D. J., Lautz, L. K., Briggs, M. A., Gordon, R. P., McKenzie, J. M. (2015). Experimental evaluation of the applicability of phase, amplitude, and combined methods to determine water flux and thermal diffusivity from temperature time series using VFLUX 2. Journal of Hydrology, 531(3), 728–737.
26. Halloran, L.J., Roshan, H., Rau, G.C., Andersen, M.S., Acworth, R.I. (2016). Improved spatial delineation of streambed properties and water fluxes using distributed temperature sensing. Hydrological Processes, 30, 2686–2702.
27. Conant, B. (2004). Delineating and Quantifying Ground Water Discharge Zones Using Streambed Temperatures. Ground Water, 42(2):243–257.
28. Alexander, M.D., Caissie, D. (2003). Variability and Comparison of Hyporheic Water Temperatures and Seepage Fluxes in a Small Atlantic Salmon Stream. Ground Water, 41(1):72–82.
29. Briggs, M.A., Lautz, L.K., McKenzie, J.M., Gordon, R.P., Hare, D.K. (2012). Using high-resolution distributed temperature sensing to quantify spatial and temporal variability in vertical hyporheic flux. Water Resources Research, 48(2), W02527.
30. Wondzell, S.M., Swanson, F.J. (1996). Seasonal and Storm Dynamics of the Hyporheic Zone of a 4th-Order Mountain Stream. II: Nitrogen Cycling. Journal of the North American Benthological Society, 15, 20–34.
31. Kalbus, E., Reinstorf, F., Schirmer, M. (2006). Measuring methods for groundwater – surface water interactions: a review. Hydrology and Earth System Sciences, 10, 873–887.

32. Fanelli, R.M., Lautz, L.K. (2008). Patterns of Water, Heat, and Solute Flux through Streambeds around Small Dams. Ground Water, 46:671–687.
33. Briggs, M.A., Lautz, L.K., McKenzie, J.M., Gordon, R.P., Hare, D.K. (2012). Using high-resolution distributed temperature sensing to quantify spatial and temporal variability in vertical hyporheic flux. Water Resources Research, 48, W02527.
34. Kasahara, T., Hill, A.R. (2006). Hyporheic exchange flows induced by constructed riffles and steps in lowland streams in southern Ontario, Canada. Hydrological Processes, 20(20):4287–4305.
35. Rosenberry, D.O., Pitlick, J. (2009). Effects of sediment transport and seepage direction on hydraulic properties at the sediment-water interface of hyporheic settings. Journal of Hydrology, 373, 377–391.
36. Taniguchi, M., Burnett, W.C., Smith, C.F., Paulsen, R.J., O'Rourke, D., Krupa, S.L., Christoff, J.L. (2003). Spatial and temporal distributions of submarine groundwater discharge rates obtained from various types of seepage meters at a site in the Northeastern Gulf of Mexico. Biogeochemistry, 66, 35–53.
37. Harvey, J.W., Böhlke, J.K., Voytek, M.A., Scott, D.T., Tobias, C.R. (2013). Hyporheic zone denitrification: Controls on effective reaction depth and contribution to whole-stream mass balance. Water Resources Research, 49, 6298–6316.
38. Edwardson, K.J., Bowden, W.B., Dahm, C.N., Morrice, J.A. (2003). The hydraulic characteristics and geochemistry of hyporheic and parafluvial zones in Arctic tundra streams, north slope, Alaska. Advances in Water Resources, 26, 907–923.
39. Anderson, W., Anderson, J.L., Thaxton, C., Babyak, C.M. (2010). Changes In Stream Temperatures In Response To Restoration Of Groundwater Discharge And Solar Heating In A Culverted, Urban Stream. Journal of Hydrology, 393, 309–320.
40. Lautz, L.K., Kranes, N., Siegel, D.I. (2010). Heat tracing of heterogeneous hyporheic exchange adjacent to in-stream geomorphic features. Hydrological Processes, 24(21):3074–3086.
41. Hatch, C.E., Fisher, A.T., Revenaugh, J., Constantz, J.E., Ruehl, C.R. (2006). Quantifying surface water–groundwater interactions using time series analysis of streambed thermal records: Method development. Water Resources Research, 42, W10410.
42. Keery, J., Binley, A., Crook, N.P., Smith, J.W. (2007). Temporal and spatial variability of groundwater–surface water fluxes: Development and application of an analytical method using temperature time series. Journal of Hydrology, 336, 1–16.
43. Stallman, R. W. (1965). Steady one-dimensional fluid flow in a semi-infinite porous medium with sinusoidal surface temperature, J. Geophys. Res., 70, 2821–2827.
44. Schmidt, C., Bayer-Raich, M., Schirmer, M. (2006). Characterization of spatial heterogeneity of groundwater-stream water interactions using multiple depth streambed temperature measurements at the reach scale. Hydrology and Earth System Sciences, 10, 849–859.
45. Shanafield, M., Hatch, C.E., Pohll, G. (2011). Uncertainty in thermal time series analysis estimates of streambed water flux. Water Resources Research, 47, W03504.
46. Liu, D., Zhao, J., Lv, H. (2017). Comparative analysis of water-heat exchange characteristics of the riparian zone downstream of dam in different seasons. Advances in Water Science. (01), 124–132.

47. Song, J., Cheng, D., Zhang, J., Zhang, Y., Long, Y., Zhang, Y., Shen, W. (2019). Estimating spatial pattern of hyporheic water exchange in slack water pool. Journal of Geographical Sciences, 29, 377–388.
48. Lautz, L.K. (2012). Heat tracing of temporal changes in vertical flux through streambed sediments. Geological Society of America Abstracts with Programs. 44(7), 50.
49. Rau, G.C., Andersen, M.S., Acworth, R.I. (2012). Experimental investigation of the thermal dispersivity term and its significance in the heat transport equation for flow in sediments. Water Resources Research, 48, W03511.
50. McCallum, A.M., Andersen, M.S., Rau, G.C., Acworth, R.I. (2012). A 1-D analytical method for estimating surface water–groundwater interactions and effective thermal diffusivity using temperature time series. Water Resources Research, 48(11), W11532.
51. Luce, C. H., Tonina, D., Gariglio, F., Applebee, R. (2013), Solutions for the diurnally forced advection-diffusion equation to estimate bulk fluid velocity and diffusivity in streambeds from temperature time series. Water Resour. Res., 49(1), 488–506.
52. Swanson, T.E., Cardenas, M.B. (2011). Ex-Stream: A MATLAB program for calculating fluid flux through sediment-water interfaces based on steady and transient temperature profiles. Comput. Geosci., 37, 1664–1669.
53. Li, Y., Zhao, J., Lv, H., Chen, B. (2016). Investigation on temperature tracer method calculated flow rate of hyporheic layer in riparian zone. Advances in Water Science. (03), 423–429.

Tables

Table 1. Experimental plan

	The water level	Head cm	Soil	Temperature ℃
Working condition 1	falling	35~20~10	homogeneous	22~30
Working condition 2	rising	10~20~35	homogeneous	22~30
Working condition 3	rising	10~20~35	heterogeneity	22~30

Table 2. Parameters of the VFLUX 2 calculation

Porosity –	Thermal diffusivity 1/m	Coefficient of heat conduction (cal·(s·cm·℃)$^{-1}$)	The specific heat capacity of water (kcal·(kg·℃)$^{-1}$)	Specific heat capacity of soil (kcal·(kg·℃)$^{-1}$)
0.41	0.01	0.00031	1.000	0.312

Figures

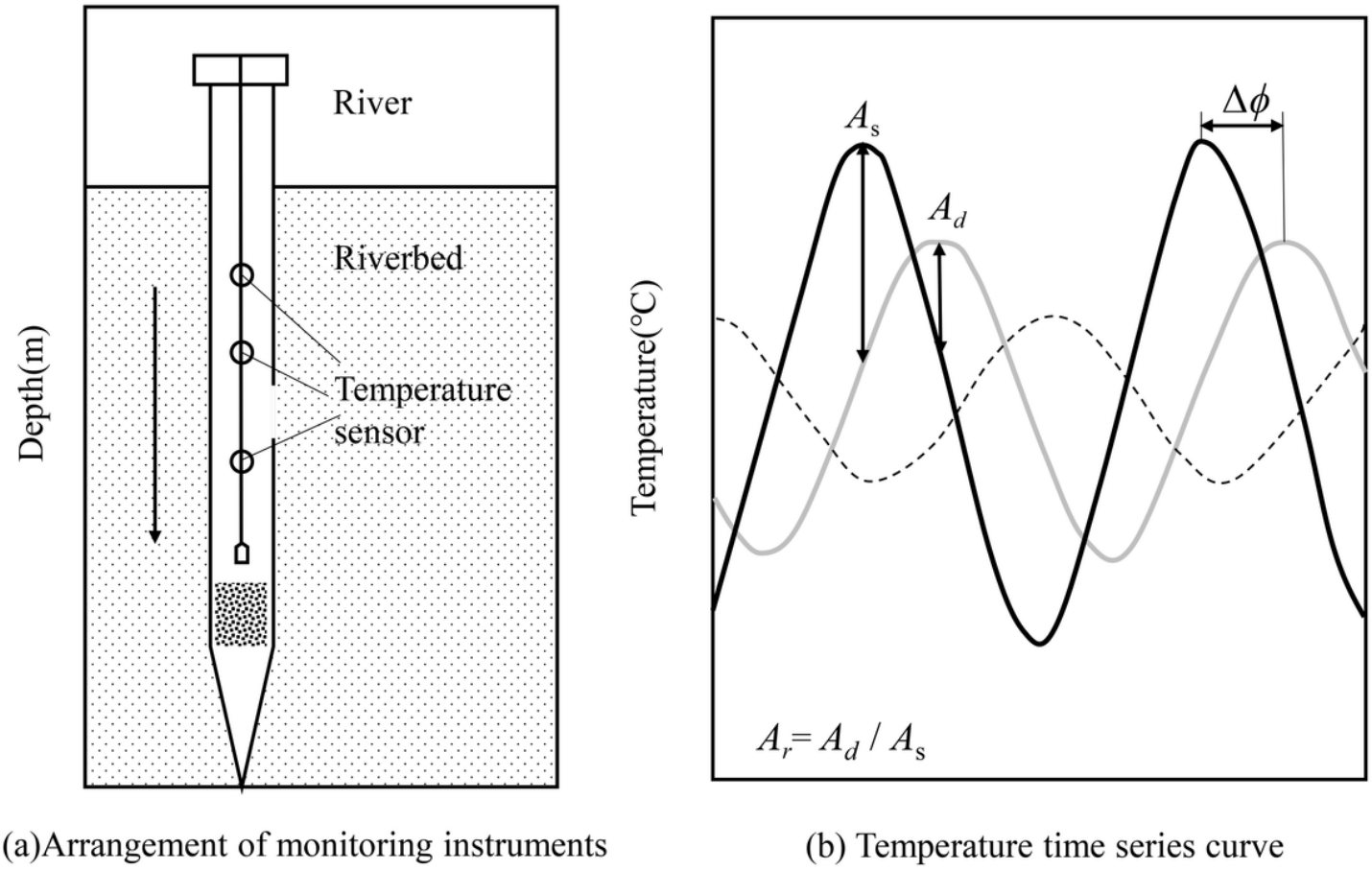

Figure 1

Sketch for the temperature time-series curves of deep and shallow measurement points and the commonly layout approaches of temperature monitoring instrument (adapted from Schmidt et al.2006)

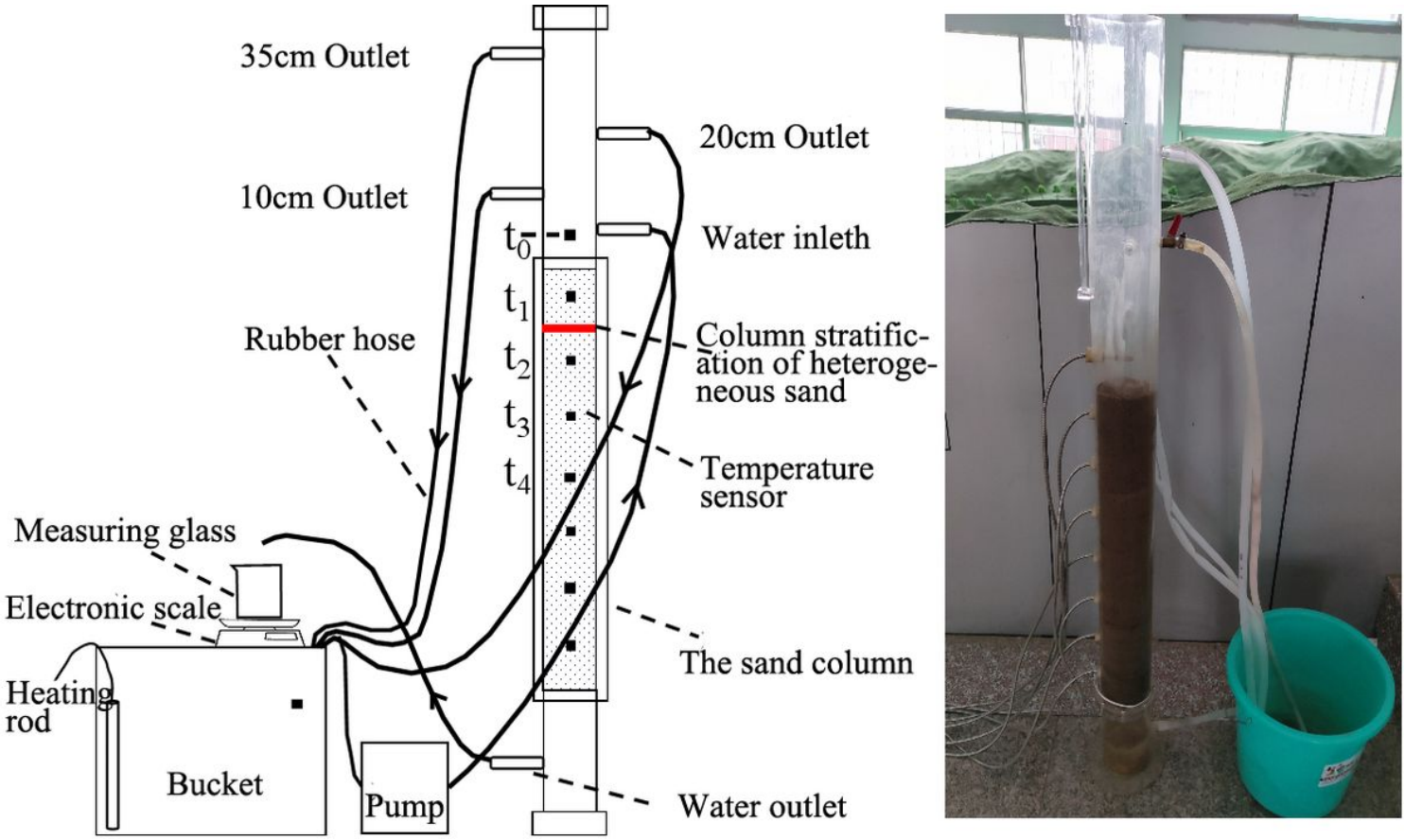

Figure 2

Experimental device schematic.

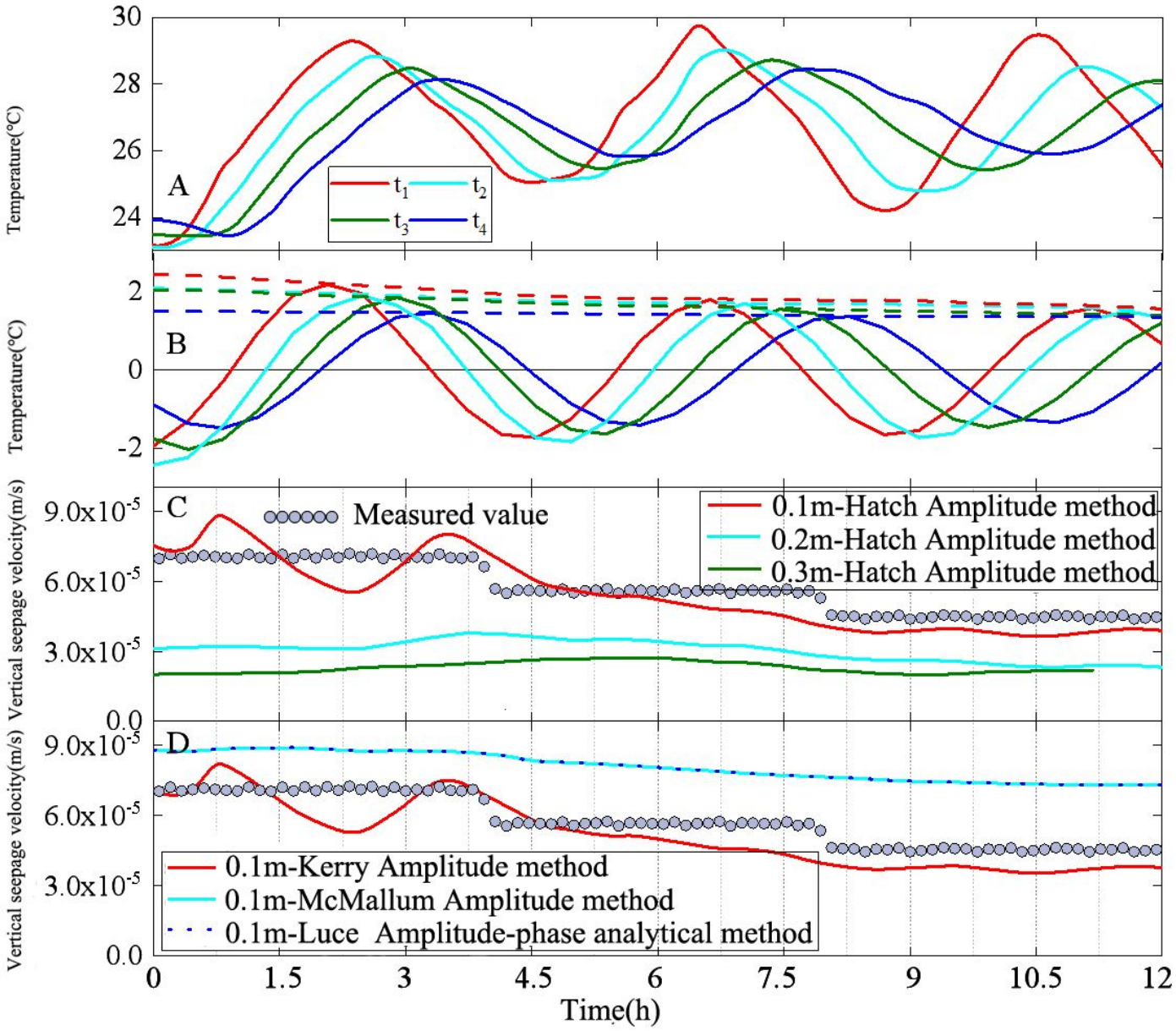

Figure 3

Variation of temperature and seepage velocity in homogeneous sand column with decreasing head(A represents the temperature change curve of each monitoring point under different water heads; B The dotted line represents the temperature amplitude of each monitoring point, the solid line represents the temperature time series data after filtering; C and D represents the vertical seepage velocity calculated by various analytic models of VFLUX2).

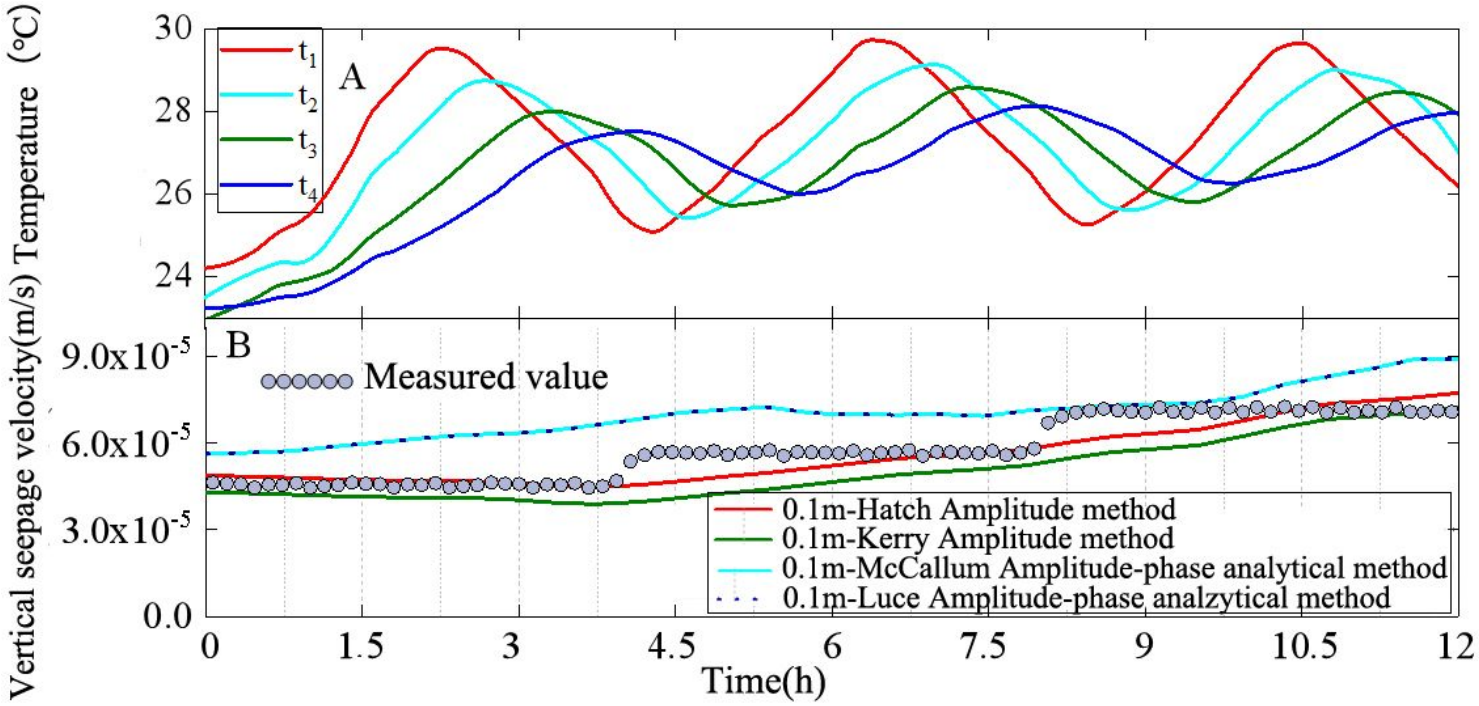

Figure 4

Variation of temperature and seepage velocity of homogeneous sand column with rising water head(A represents the temperature change curve of each monitoring point under different water heads; B represents the vertical seepage velocity calculated by various analytic models of VFLUX2).

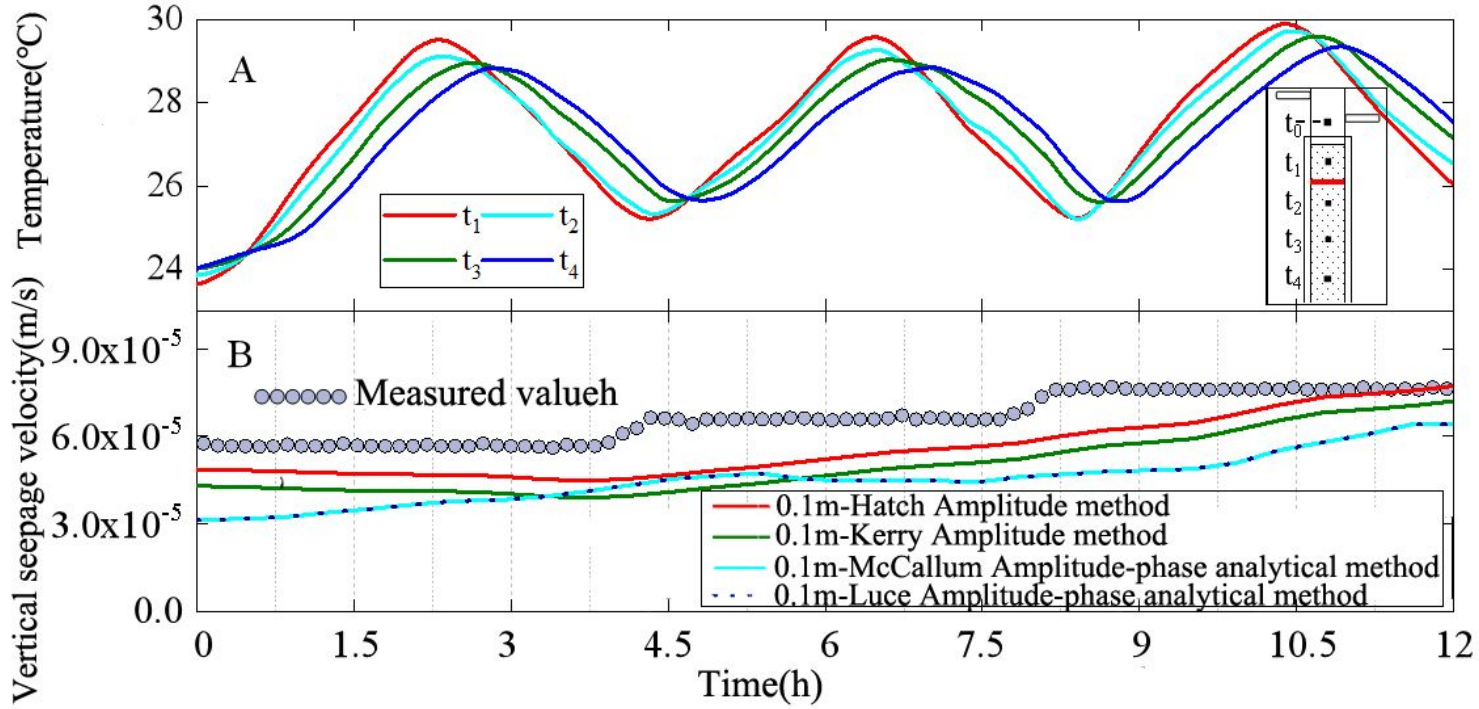

Figure 5

Variation of temperature and seepage velocity of heterogeneous sand column with rising water head(A represents the temperature change curve of each monitoring point under different water heads; B represents the vertical seepage velocity calculated by various analytic models of VFLUX2).